Updated Harmonic and Interharmonic Current Summation Rule in Wind Power Plants with Type III Wind Turbines

Hamed Ghanavati
Department of Electrical Engineering
Iran University of Science and Technology (IUST)
Tehran, Iran
h_ghanavati@elec.iust.ac.ir

Łukasz H. Kocewiak
Electrical System Design and Grid Integration
Ørsted Offshore Wind
Gentofte, Denmark
lukko@orsted.dk

Alireza Jalilian
Department of Electrical Engineering
Iran University of Science and Technology (IUST)
Tehran, Iran
jalilian@iust.ac.ir

***Abstract*—An assessment of Wind Turbine (WT) harmonic current contribution to the grid (Primary Emission, PE) at the Wind Power Plant (WPP) Point of Connection (PoC) is presented in this paper. Also, the contribution of the grid background harmonic voltage distortion to the harmonic current distortion at the WT terminals (Secondary Emission, SE) is evaluated. The procedure is carried out based on PE Transfer Function (TF) and SE Transfer Admittance (TA). To increase the accuracy of these TFs in studying harmonic current summation in WPP harmonic assessment procedure, the TFs must also include the Doubly-Fed Asynchronous Generator (DFAG)-based WT impedance. Hence, this article proposes a new model of PE TFs and SE TAs including the type III WT impedance. The proposed approach includes average modelling of DFAG back-to-back converters to extract the total impedance of the WT (including passive components and converter equivalent impedance) within its linear operating range. Moreover, the application of harmonic summation formula from IEC 61000-3-6 in WPP's harmonic studies can provide unreliable results because this standard ignores the phase angle variation of complex harmonic currents. Hence, the detailed studies are done in time and frequency domains to provide adjusted α-exponent to the IEC 61000-3-6 summation rule. To validate the outcome, three different analysis methods are used and compared: (i) frequency domain model based on new TFs; (ii) time domain model based on detailed dynamic simulations performed in MATLAB/SIMULINK where different Power Bins (PBs) are assigned to WTs; (iii) harmonic current source model according to the IEC 61000-3-6 summation rule with standard and adjusted α-exponents.**

Keywords—Wind turbine, Harmonic, Primary and secondary emission, Transfer function, Resonance, Phase angle distribution, IEC 61000-3-6 summation rule.

I. INTRODUCTION

Among renewable energy sources, wind power has highest contribution to global electricity production after hydro-power sources. Wind power capacity has experienced 11% growth over the past year; i.e., 52 GW added globally in 2017. Cumulative capacity from this source is around 539 GW [1].

Wind Turbines (WTs) are classified into fixed-speed and variable (or adjustable)-speed [2]. Fixed-speed WTs in which the turbine's rotor speed is fixed by the supply grid frequency, have some disadvantages like uncontrollable reactive power consumption, the limited efficiency and the need for a gear box [2]. In modern variable-speed WTs it is possible to control rotor speed through power electronic converters [2, 3].

Doubly-Fed Asynchronous Generator (DFAG)-based variable-speed WTs (called type III WTs) are equipped with reduced-capacity power converters [3, 4] and Permanent Magnet Synchronous Generator (PMSG)-based variable-speed WTs (called type IV WTs) are equipped with full-capacity power converters [5]. The switching of converters produces harmonic [6] and interharmonic [5] and also results in WT active output power distortions [4, 7]. These harmonics have a stochastic behaviour during the time and vary based on WT operating point, converter control scheme and switching pattern [7].

Harmonic interactions of Wind Power Plants (WPPs) with the external grid and harmonic propagations through collection grid are known as power quality problems [2]. Also, harmonic amplifications within WPP electrical infrastructure due to resonances mainly between transformers inductance as well as submarine and underground transmission cables capacitance can cause excessive power quality problems [3, 8]. Two main harmonic problems related to grid-connected WPPs are harmonic emission and harmonic resonance [9]. Harmonic current emissions propagated through the WPP electrical infrastructure are classified into Primary Emission (PE) and Secondary Emission (SE) [10]. It has been reported that harmonic currents emitted by WTs in a WPP (or PE) transfer to the grid at some frequencies with larger amplitude after applying the IEC summation formula [6, 11-14]. Also, the grid can contribute to harmonic distortion and can be modelled as a background harmonic voltage source which can separately cause harmonic current flow (or SE) at the WPP's Point of Common Coupling (PCC) [10]. The total harmonic current at PCC is the combination of these two types of emissions [10, 11, 15].

Accurate measurements of harmonics and interharmonics at PCC and also the correlation of harmonic/interharmonic groups with WT active output power are well represented in [2-5, 7, 15]. Although, as expected, the major part of total harmonic current at PCC is due to SE; Thus, the measurements of current at this point does not provide exhaustive information about PE itself. The method used to decompose these two types of emissions is based on the concept of Transfer Function (TF) and is addressed in [10, 15]. The contribution of each WT harmonic current to the total harmonic current at the WPP's Point of Connection (PoC) can be calculated using PE TF. Also, the contribution of grid background harmonic voltage distortion to the harmonic current distortion at the WT terminals can be calculated using SE Transfer Admittance (TA) [2, 11,15].

In order to extract TFs and to investigate the WPP resonances based on these TFs, the harmonic model of WPP components is required in frequency domain [2, 6, 9]. In [14], a network reduction method is proposed for reducing detailed model of WPP. A detailed model of WPP is

presented in [16] to study the resonances phenomena. These publications, based on IEC 61400-21, assume the WT current spectrums as an array of ideal harmonic current injection sources neglecting the internal impedance of the WT [17]. The analysis performed in [8] shows the WT equivalent circuit for evaluating series and parallel resonances with considering WT generator impedance and then the proposed harmonic model of WT grid-connected is validated; but a method that extracts the WT impedance has not been presented in it.

Two recent methods for extracting DFAG impedance are average modelling method and sequence modelling method. Sequence impedance modelling method is valid from sub-synchronous frequency up to 1/3 of the converter switching frequency [18]. It is desirable to derive a model that is accurate enough for analysing harmonic interactions up to 2.5 kHz (i.e. 50^{th} harmonic in the 50-Hz systems) and for achieving the same results as a detailed switching circuit model when the switching frequency is much higher than the frequency of interest. The average modelling method is presented in [19-21] to calculate the inverter impedance of a Distributed Generation (DG) source with considering converter control structure. Average modelling method is well represented in [22-24] for type III WTs (including harmonic model of back-to-back converters, LCL filter, and generator harmonic equivalent circuit) and in [25] for type IV WT back-to-back converters. The accuracy of the average modelling method to calculate DFAG impedance has been validated by [22, 23] up to 2.5 kHz. In [26, 27], the output impedance of type III and type IV WTs is represented for Sub-Synchronous Control Interaction (SSCI) studies. Also, an overview on methods for harmonic resonance analysis and modelling of WT power converters is performed in [28]. None of the mentioned literatures have applied obtained WT output impedance to TF models for studying PE and SE. Hence, in this article, DFAG rotor part (including Rotor Side Converter, RSC and Asynchronous Generator, AG) and grid part (including Grid Side Converter, GSC and LCL filter) are extracted based on average modelling method. Moreover, the novelty of this work is the application of updated impedance models for TF analysis. The design process of LCL filter described in [29] is used in this paper.

After extracting the converters' impedance, they must be included in the harmonic model of WPP's other components (such as transformers, underground transmission cables, external grid, etc.). This is carried out by considering Norton/Thévenin equivalent circuit for grid-connected WT system. Thévenin equivalent circuit of the type III WT is presented in [8, 17, 22, 23, 27, 28]. Norton equivalent circuit of the type IV WT is presented in [30]. The validation of the Norton/Thévenin models for evaluating the series and parallel resonances is verified in [8, 22, 23]. A comparison between average model, switching model, and Norton model is done in [20] and the validation of grid-connected WT Norton model and DG inverter average model is verified in it. If there are *N* WTs in a WPP, then the total TF is equivalent to the TFs of all WTs together at a specific node [15]. Harmonic aggregation comes from here. Such an aggregation effect will increase the harmonic current levels transferred to PCC especially at resonance frequencies reflected in the TF. The greatest impact on the network and adjacent installations will occur at these frequencies. The phase angle distribution becomes important when studying the aggregation effect. Since the phase angles of complex harmonic currents are not considered in IEC 61400-21 (and also IEC TR 61000-3-6) summation rule, the application of this rule to harmonic and interharmonic groups can provide unreliable results in WPP's harmonic studies. Phase angles of different harmonic components have different distributions at low and high frequencies [6]. Two aggregation cases for harmonic phase angles are presented in [11]: (1) "identical" harmonic phase for all harmonic sources; (2) harmonic phase with "uniform" distribution for all harmonic sources. The results of studies performed in [11] show that the total PE at PCC for case (1) aggregates with the number of WTs, and for case (2) aggregates with the square root of the number of WTs. The problem regarding to the analysis of the aggregation factor in [11, 15] and the phase angle distribution in [6] is that they do not consider WT impedance in TFs. It is worth emphasizing that harmonic interactions between the grid and WT converters can introduce new resonances in TFs that in turn can affect harmonic aggregation behaviour and summation as presented in [6, 12-14]. Hence, as second contribution, this article is aimed to applying updated TFs to WPP's Norton model in order to adjust α-exponent in IEC 61000-3-6 summation rule. To do so and to validate the outcome, three different analysis methods are used and compared: (i) frequency-domain model (or circuit model) to perform TF-based harmonic propagation studies including the detailed modelling of type III WT; (ii) time-domain model (or simulation model) to perform harmonic propagation studies based on detailed dynamic simulations performed in MATLAB/SIMULINK where different WT's operating points are considered; (iii) harmonic current source model to perform harmonic propagation studies according to the IEC 61000-3-6 summation rule with standard and adjusted α-exponents.

Harmonic current spectrums as input data for harmonic current injection source in Norton model are monitored at the MV side of a type III WT transformer simulated in MATLAB/SIMULINK under different wind conditions. The Power Bin (PB) concept according to IEC 61400-21 and grouping method according to IEC 61000-4-7 are applied to these spectrums. The contribution of SE to the monitored currents at measuring point is zero. The current measured as input for the aggregation studies in this paper is PE only.

In this regard, average modelling of the type III WT is introduced in section II. In section III, circuit models for harmonic TFs and TAs in presence of the WT system impedance are extracted. In order to validate the circuit models, a comparison with time-domain simulations is made in section IV. Time- and frequency-domain models obtained in previous sections are assessed to update harmonic summation rule in section V. Conclusions and some recommendations are presented in section VI.

II. Type III WT Average Modelling

Due to the widespread use of power electronic devices and feedback controllers in WPPs, the Thévenin impedance does not only consist of passive components of WT (e.g. series reactor, shunt harmonic filter, generator windings, transformer, etc.), but also the internal impedance of GSC defined by control schema and operating points [17, 30]. The origin of harmonic problems in WPPs is the combination of WT harmonic contribution and the resonant characteristic of WPP impedance which causes significant harmonic distortion at the point of interest. Depending on the inverter design and grid parameters, harmonic resonances may also appear within the inverter control

bandwidth range. This is the desired frequency range in which the impact of inverters harmonic distortion is studied.

Voltage Source Converter (VSC) used in DFAG may has a very low harmonic impedance (in its linear working range; i.e. from 150 Hz up to 2.5 kHz) and, due to its frequency dependency, cannot be accurately represented by an ideal current source. Hence, in [8, 13, 17, 30] a Thévenin/Norton equivalent is proposed whereby frequency dependency of equivalent parallel/series impedance can be modelled accurately. In addition to that, since the harmonic filters used in DFAGs are resonant circuits typically tuned to attenuate high frequencies, their resonance profile should also be considered in the Norton/Thévenin impedance. An example of harmonic representation of a DFAG based on [8, 13, 17, 30] is illustrated in Fig. 1. "Thévenin-based DFAG Equivalent Circuit" determines that each DFAG part (rotor part and grid part) is modelled as an equivalent circuit based on Thévenin theorem. Then, these two parts are paralleled together to obtain WT impedance. The WT harmonic current injection is then used as a current source in parallel with the WT impedance based on Norton theorem to obtain the harmonic model of a grid-connected WT.

DFAG modelling in accordance to [24] is as follows: (i) GSC harmonic current flows through the LCL filter and WT transformer to the grid, (ii) harmonics produced by RSC are propagating from the rotor to the stator and then transmitted to the grid; see Fig. 2.

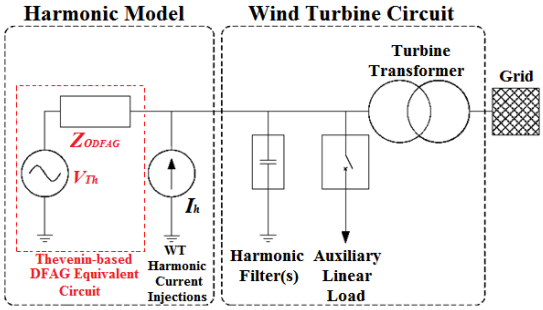

Fig. 1. Harmonic model of a DFAG based on [8, 13, 17, 30].

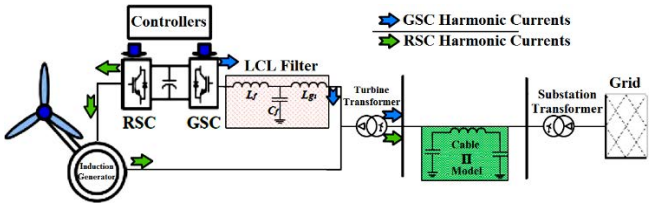

Fig. 2. Single-line diagram of a type III grid-connected WT.

A. GSC and LCL-filter Modelling

GSC is responsible for controlling the DC-link capacitor voltage and reactive power flow to the grid. The GSC current closed-loop control is modelled based on Thévenin theorem as voltage source and impedance in series [22, 23], as shown in Fig. 3. According to [24], the Proportional-Resonant (PR) regulator is used to control the LCL filter output current, i_{g1}, as well as proportional gain of inner loop for controlling LCL filter capacitor current, i_{cf} [20].

The TF of PR controller is expressed as:

$$G_{GSC}(s) = k_p + k_i \frac{s}{s^2 + \omega_0^2} \quad (1)$$

In (1), the k_p and k_i are proportional and integral gains respectively and their values are equal to 1 and 2000 respectively, based on [24]. ω_0 is the angular frequency equal to the power system fundamental frequency. It is worth mentioning that the dynamics of the outer power control and and synchronization loops are usually characterized by much slower dynamics than the inner current control loop [20], which may cause oscillations around the fundamental frequency (i.e. sub- and super-synchronous). However, the outer control loops can be neglected within the harmonic frequency range of interest for the sake of simplicity, and only the interactions between the current control loops of the converter with the passive components are investigated in this paper. Also, for the linearization of the average circuit model, the dc-bus voltage is assumed to be constant.

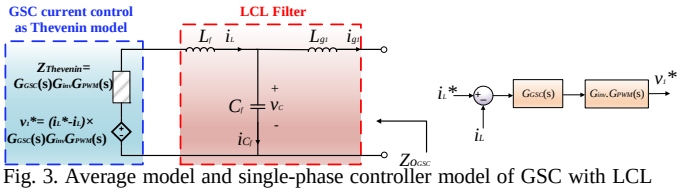

Fig. 3. Average model and single-phase controller model of GSC with LCL filter based on [22, 23].

The TF of PWM-based Voltage Source Inverter (VSI) is modelled as a delay with time constant (T_d) equal to 1.5 times the sampling period (T_s=1/f_s; where sampling frequency, f_s, is equal to 256 times the power system frequency):

$$G_{PWM}(s) = e^{-T_d s} = e^{-1.5T_s s} \approx \frac{1 - 0.75T_s s + 0.1875T_s^2 s^2}{1 + 0.75T_s s + 0.1875T_s^2 s^2} \quad (2)$$

In (2), the Padé approximation method is used to approximate exponential function e^{-Tds}. In order to generate the voltage v_1^*, the above TF must also be multiplied by G_{inv} (the ratio of DC-link voltage to the magnitude of carrier waveform). This value is equal to 250 as mentioned in [24]. The impedance of GSC and LCL filter seen from the PCC can be obtained by setting the voltage source to zero in Fig. 3.

B. RSC and AG Modelling

The RSC, which is responsible for controlling active and reactive power flowing from AG to the grid, uses the vector control method [19] here as well as the Proportional-Integral (PI) controller [22-24]. In a typical RSC controller, the inner loop controls the current and the outer loop controls the power; but as mentioned in section II-A, the outer control loops are ignored in this paper. RSC model in DFAG system is shown in Fig. 4.

The RSC current closed-loop control is modelled based on Thévenin theorem as voltage source and impedance in series. The TF of PWM-based VSI is as (2). In Fig. 4, ς corresponds to the slip. TF of the PI controller is:

$$G_{RSC}(s) = k_p + \frac{k_i}{s} \quad (3)$$

In (3), values of k_p and k_i are given as 1.8475 and 21130 respectively in [24]. The impedance of RSC and AG seen from the PCC can be obtained by setting the rotor control voltage source to zero in Fig. 4.

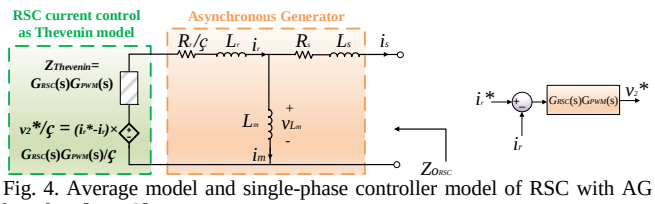

Fig. 4. Average model and single-phase controller model of RSC with AG based on [22, 23].

C. Back-to-back Converter Modelling

With respect to the fact that both converters are parallel to each other, DFAG back-to-back converter model is as Fig. 5. The equivalent impedance of GSC segment (Z_{oGSC}(s)), according to Fig. 5, is as follows:

$$Z_{o_{GSC}}(s) = Z_{L_{g1}}(s) + \left.\frac{v_c}{-i_{g_1}}\right|_{i_1^*=0}$$
$$= Z_{L_{g1}}(s) + \left(Z_{C_f}(s) \middle\| \left(Z_{L_f}(s) + \left.\frac{v_1^*}{-i_L}\right|_{GSC\ Control\ Block}\right)\right) \quad (4)$$
$$= Z_{L_{g1}}(s) + \left(Z_{C_f}(s) \middle\| \left(Z_{L_f}(s) + G_{GSC}(s) G_{inv} G_{PWM}(s)\right)\right)$$

and the equivalent impedance of RSC segment (Z_{oRSC}(s)), according to Fig. 5, is as follows:

$$Z_{o_{RSC}}(s) = Z_s(s) + \left.\frac{v_{L_m}}{-i_s}\right|_{i_2^*=0}$$
$$= Z_s(s) + \left(Z_{L_m}(s) \middle\| \left(Z_r(s) + \left.\frac{v_2^*/\varsigma}{-i_r}\right|_{RSC\ Control\ Block}\right)\right) \quad (5)$$
$$= Z_s(s) + \left(Z_{L_m}(s) \middle\| \left(Z_r(s) + G_{RSC}(s) G_{PWM}(s)\right)\right)$$

Subsequently, the equivalent impedance of DFAG segment (Z_{oDFAG}(s)) is as follows:

$$Z_{o_{DFAG}}(s) = Z_{trf}(s) + \left(Z_{o_{GSC}}(S) \middle\| Z_{o_{RSC}}(S)\right) \quad (6)$$

In (4) and (5), $Z_{Lf} = sL_f$ is the inductor impedance of the GSC LCL filter, $Z_{Lg1} = sL_{g1}$ is the grid side inductor impedance of LCL filter, $Z_{Cf} = 1/(sC_f)$ is the capacitor impedance of LCL filter, $Z_S = R_S + sL_S$ is the stator impedance, $Z_r = (R_r/\varsigma) + sL_r$ is the rotor impedance, $Z_{Lm} = sL_m$ is the magnetizing impedance, and $Z_{trf} = R_{trf} + sL_{trf}$ is the WT transformer impedance.

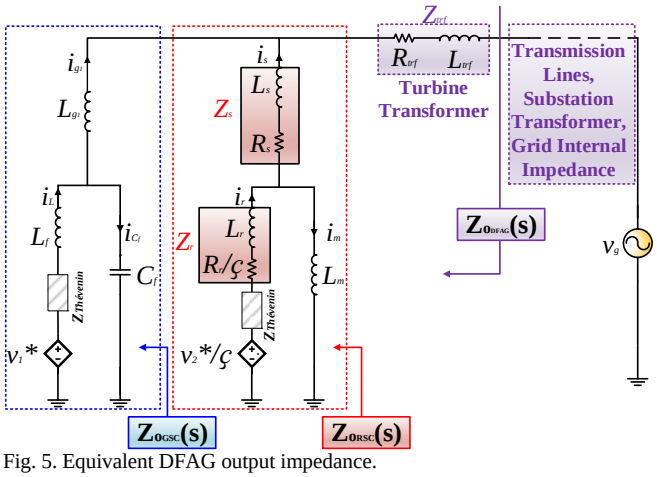

Fig. 5. Equivalent DFAG output impedance.

III. Circuit Models for Harmonic Transfers

In order to study the harmonic propagation in a systematic way, their classification into two groups is suggested by [10, 15]: Primary Emission (PE) and Secondary Emission (SE). PE is the emission from a typical harmonic source; for example, emission from an individual WT to PCC, or to another WT. SE originates from other locations; for example, emission propagating from the grid to each WTs or to PCC.

A. Studied WPP

According to Fig. 6, the WPP consists of 10 type III WTs with 2 MW of rated power each, which is distributed over two feeders symmetrically. The assumptions taken by [2, 10] about the harmonic model of underground cables, turbine and substation transformer, and the external grid are also adopted here. If R_f is the resistance at the frequency f and R_1 is the resistance at power system frequency f_{nom}, then the frequency dependency of the cable resistance is modelled as:

$$\frac{R_f}{R_1} = (1 - a_c) + a_c \times \left(\frac{f}{f_{nom}}\right)^{b_c} \quad (7)$$

In (7), damping factor of frequency-dependent resistance is b_c and a_c is a coefficient and its value is obtained from skin effect sensitivity analysis [10]. In this paper a_c is equal to 1.

In each feeder, the distance between adjacent WTs is approximately 320 meters. A 32-kV collection grid is connected to the grid through the substation transformer (30 MVA with 10% impedance, X/R ratio of 12, and damping factor b_c of frequency-dependent resistance equal to 1). WTs are connected together via underground cables (modelled using nominal Π representation with damping factor of frequency-dependent resistance equal to 0.6) with a resistance of 0.13 at 50 Hz, capacitance of 0.25 F/km, and inductance of 0.356 mH/km. It should be stated that each WT is connected to the underground cables through a WT transformer (2.5 MVA with 6% impedance, X/R ratio of 8.34, and damping factor of frequency-dependent resistance equal to 1). The substation transformer is of 110-kV and the grid has a fault level of 1716 MVA with internal impedance (R_{grid} + jX_{grid}) of 0.604+j0.0604 pu, and damping factor of frequency-dependent resistance equal to 0.8. The values of rotor resistance (R_r), reactance (X_r), and slip (ς) are 0.0389 pu, 0.085 pu, and 0.7 pu respectively. Also, the values of stator resistance (R_S) and reactance (X_S) are 0.005 pu and 0.179 pu respectively. The magnetizing reactance (L_m) is 7.089 pu and the damping factor of stator frequency-dependent resistance is 0.8 based on [10].

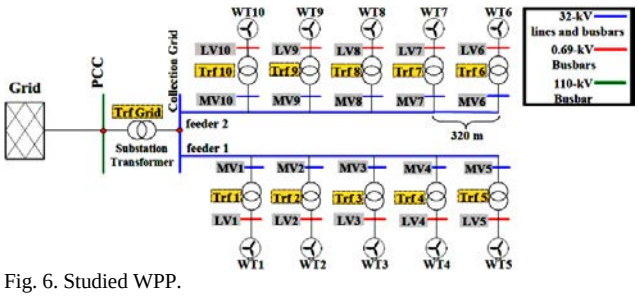

Fig. 6. Studied WPP.

B. Primary Emission Transfer Function (PE TF)

TF is defined as ratio of harmonic current at an output node (here, PCC) and a harmonic current source (here, WT) for determining the contribution of each WT to the obtained total PE at PCC. To do so, the other WTs are open circuit and then, the PE TF of studied WT is calculated. In fact, in calculating the PE TF from a studied WT, it is assumed that the impact of SE from other WTs is negligible.

The equivalent circuit used to study PE TF from a single WT (here, WT1 from Fig. 6) to the grid is shown in Fig. 7. The cable between the studied WT in one feeder and the PCC is labelled as "segment 1"; the rest of the cable between that WT and the end of the same feeder is labelled as "segment 2"; and the other feeder cable is labelled as

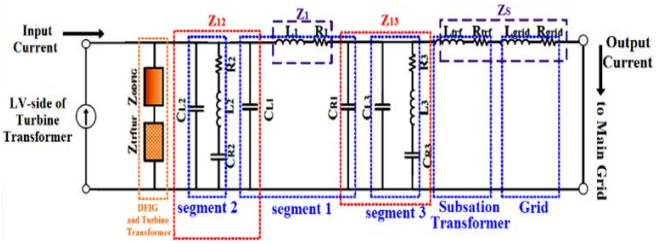

Fig. 7. Equivalent circuit of PE TF from WT1 to the grid.

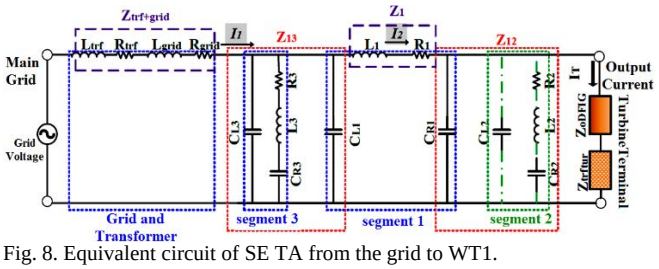

Fig. 8. Equivalent circuit of SE TA from the grid to WT1.

"segment 3". Z_S represents the equivalent impedance of substation transformer and the grid internal impedance, and Z_1 represents the equivalent impedance of series part of "segment 1". Each cable according to Fig. 7 has two capacitors: left-half capacitance (C_L) and right-half capacitance (C_R) that are equal. C_{L1}/C_{R1} is the left-/right-half capacitance of the cable located between studied WT in one feeder and PCC; C_{L2}/C_{R2} is the left-/right-half capacitance of the cable located between the studied WT and the end of the same feeder to which the WT is connected; and C_{L3}/C_{R3} is the left-/right-half capacitance of the other feeder cable. Z_{12} represents the equivalent impedance of "segment 2" parallel with left-half capacitance of "segment 1"; Z_{13} represents the equivalent impedance of "segment 3" parallel with right-half capacitance of "segment 1"; and Z_{trftur} is the equivalent impedance of turbine transformer from its MV-side. TF, as ratio of output and input current, is:

$$H_{WT,Grid}(\omega)=\frac{Z_{13}}{Z_{13}+Z_s}\times \frac{Z_{12}\left\|(Z_{o_{DFIG}}+Z_{trftur})\right.}{(Z_{12}\left\|(Z_{o_{DFIG}}+Z_{trftur})\right.)+Z_1+\frac{Z_{13}\times Z_s}{Z_{13}+Z_s}} \quad (8)$$

It is worth mentioning that in "segment 1" (as Π-model of the cable feeder between WT1 and PCC), WT1 is sender of current and PCC is receiver. But, in both "segments 2, 3" the WT is emitting current but there is no receiver because, as noted earlier, other WTs are open circuit. Hence, the receiver side is open circuit and $C_{R2(3)}$ will be in series with $L_{2(3)}$+$R_{2(3)}$.

C. Secondary Emission Transfer Admittance (SE TA)

TA assesses the impact of background voltage distortion, which propagates from the grid, on the current obtained at the WT terminals due to this distortion. The equivalent circuit used to calculate the SE TA from the grid to WT1 is shown in Fig. 8. "Segment 1" and "segment 3" are defined as in section III-B. The remaining cables existing in common feeders with the studied WT, are labelled as "segment 2"; if the studied WT is end-of-feeder turbine, then this segment will be ignored. For WT1, "segment 2" is cable between WT1 and WT5. Z_1 represents the equivalent impedance of series part of "segment 1". Z_{12} represents the equivalent impedance of "segment 2" parallel with right-half capacitance of "segment 1"; Z_{13} represents the equivalent impedance of "segment 3" parallel with left-half capacitance of "segment 1"; and $Z_{trf+grid}$ is the equivalent impedance of transformer and the grid internal impedance.

TA, as ratio of output current and input voltage, is:

$$Y_{Grid,WT4}(\omega)=\frac{Z_{12}}{Z_{gT}\times(Z_{12}+Z_{trftur}+Z_{o_{DFIG}})}\times \frac{Z_{13}}{Z_{13}+Z_1+\frac{Z_{12}\times(Z_{trftur}+Z_{o_{DFIG}})}{Z_{12}+Z_{trftur}+Z_{o_{DFIG}}}} \quad (9)$$

In (9), Z_{gT} is total wind farm impedance which is equal to:

$$Z_{gT}=Z_{trf+grid}+\frac{\left(\frac{(Z_{trftur}+Z_{o_{DFIG}})\times Z_{12}}{Z_{trftur}+Z_{o_{DFIG}}+Z_{12}}+Z_1\right)\times Z_{13}}{\left(\frac{(Z_{trftur}+Z_{o_{DFIG}})\times Z_{12}}{Z_{trftur}+Z_{o_{DFIG}}+Z_{12}}+Z_1\right)+Z_{13}} \quad (10)$$

IV. Simulation Results and Circuit Models Validity

Table I shows the parameters of LCL filter designed for converters simulation. The filter design procedure is given in detail in [29]. Taking into consideration this table and (6), the DFAG output impedance (magnitude and phase) is shown in Fig. 9. Interaction of back-to-back converters results in new parallel resonance frequencies at 175 Hz and 995 Hz with magnitudes of 104 Ω and 4 Ω in DFAG output impedance respectively, while parallel resonance frequency of RSC is 315 Hz with magnitude of 61 Ω and GSC does not

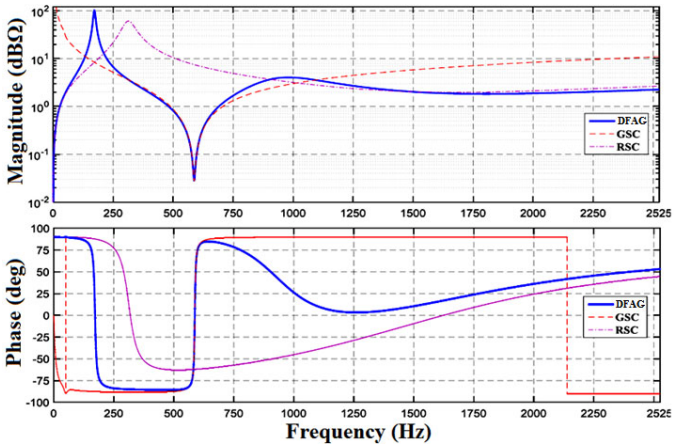

Fig. 9. Magnitude and phase of DFAG, GSC, and RSC output impedance.

TABLE I
Required Parameters for LCL Filter Design Based on [24] for Converters Simulation

	Parameter	Value
LCL Filter	GSC-side inductor (L_f)	1 mH
	Capacitor (C_f)	100 μF
	Grid-side inductor (L_{g1})	0.73 mH
	Converter switching frequency	1950 Hz
	DC-link capacitance	20000 μF
	DC-link voltage	1200 V

show a significant parallel resonance. However, it shows a very prominent series resonance due to the LCL filter.

In following, the frequency response of PE and SE circuit models presented in sections III-B, C is plotted and validated by comparison with time-domain results.

A. *Frequency Response of PETF and SETA Circuit Models*

The diagram of $|H_{WT,\,Grid}\,(\omega)|$ according to (8) is plotted in Fig. 10 up to 2.5 kHz for two cases: "with average modelling" and "without average modelling" of the DFAG converter system. In case "with average modelling", the first resonance frequency occurs at 175 Hz which is in accordance with the first resonance of DFAG impedance. At frequencies below 500 Hz the PE TF value in case "without average modelling" is around 1, while for case "with average modelling" it is about 0.85. The maximum value of TF for PE is at 1585 Hz with magnitude of 14.66, while this level reaches to 11.22 at 1715 Hz by using the DFAG average modelling: an increase in resonance frequency and a decrease in transfer level.

The cable to which the WT is connected determines the parallel resonances. The parallel resonances (at 1585 and 1715 Hz) occur when the absolute value of denominator of the lower fraction of (8) reaches its minimum. A parallel resonance results in high harmonic voltage distortion at the WPP connection point to the public grid. The influence of the converter controller reflected by the average model is visible below the switching / Nyquist frequency. At frequencies higher than 2.5 kHz it is expected that the passive components will be visible in the frequency characteristic and the impedance exhibits passive and inductive behaviour.

Fig. 11 shows the diagram of $|Y_{Grid,\ WT1}\ (\omega)|$ in logarithmic scale (base 10) according to (9) and (10) up to

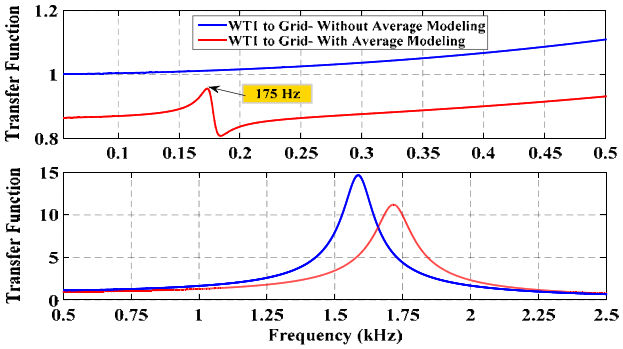

Fig. 10. PE TF from WT1 to the grid with and without converter average modelling. Upper figure: 0-0.5 kHz; lower figure: 0.5-2.5 kHz.

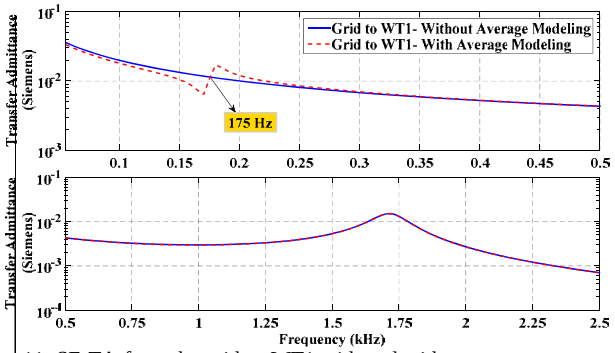

Fig. 11. SE TA from the grid to WT1 with and without converter average modelling. Upper figure: 0-0.5 kHz; lower figure: 0.5-2.5 kHz.

2.5 kHz for two cases; "with average modelling" and "without average modelling" of the DFAG converter system. Similar to the section IV-A, in case "with average modelling", first resonance frequency occurs around 175 Hz which is in accordance with the first parallel resonance of the DFAG impedance. The maximum level of TA for case "without average modelling" is at 1715 Hz with magnitude of 0.0152 S. In this emission class, the average modelling does not affect the maximum level of TA and its corresponding resonance frequency.

The series resonances due to all other cables and the transmission transformer occur at frequency range between 20-50 kHz. Since the average modelling method is valid only for frequencies up to 2.5 kHz, it is not adequate to show series resonances in Figs 10, 11.

B. *Time-domain Results of PE TF and SE TA*

In order to validate the proposed circuit models of PE TF and SE TA, the simulation of a WT presented in Fig. 2 is performed in the MATLAB/Simulink. WT (as harmonic current injection source) is in 40 % Power Bin (PB) for PE studies (for PB concept; see IEC 61400-21). In addition, the grid is modelled as a voltage source for the SE studies. The indicated planning levels of voltage harmonics from the standard IEC 61000-3-6 are used as voltage emission levels for harmonic frequencies, and 0.2% of nominal voltage is used for interharmonic frequencies [10]. The comparison of time-domain results with analytical calculations ((8), (9)) of circuit models (Figs. 10, 11) is presented in Fig. 12 for PE and in Fig. 13 for SE. All spectrums have been derived with Discrete Fourier Transform (DFT) in MATLAB for each 10-cycle waveform, resulting in a complex current for each

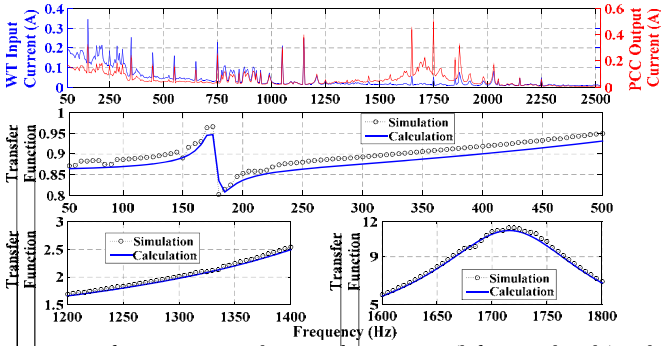

Fig. 12. PE from WT1 to grid. Upper figure: Input (left vertical scale) and output current spectrum at PCC (right vertical scale). Middle and bottom figures: TF obtained from simulations (ratio of output and input currents) and circuit model.

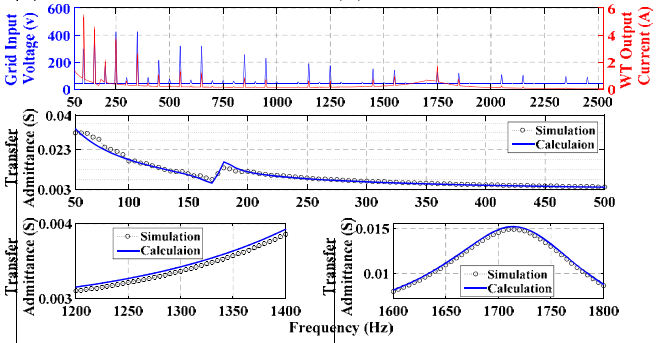

Fig. 13. SE from grid to WT1. Upper figure: Input voltage spectrum (left vertical scale) and output current spectrum at WT terminal (right vertical scale). Middle and bottom figures: TA obtained from simulations (ratio of output current and input voltage) and circuit model.

5-Hz resolution component. Grouping method according to IEC 61000-4-7 are applied to these spectrums.

Monitored harmonic current distortion at PCC due to WT harmonic currents (blue-line curve with left vertical scale at upper figure of Fig. 12) is shown in upper figure of Fig. 12 (red-line curve) with right vertical scale. By dividing these two spectrums, PE TF will be obtained. The results are shown in middle and bottom figures of Fig. 12. The simulation model has only a slight deviation from calculation model around 170 Hz that is negligible. Also, monitored harmonic current distortion at WT terminal due to grid background voltage harmonic distortion (blue-line curve with left vertical scale at upper figure of Fig. 13) is shown in upper figure of Fig. 13 (red-line curve) with right vertical scale. By dividing these two spectrums, SE TA will be obtained. The results are shown in middle and bottom figures of Figure 13. The results show that the simulation model has well tracked the calculation model.

V. Harmonic Summation: Adjusting α-Exponent

A general law for summation of harmonic current from different harmonic sources is presented in IEC 61000-3-6. According to this law, the magnitude of the resulting harmonic current (I_h) at a certain place at order h, considering the aggregation of N harmonic sources, is:

$$I_h = \sqrt[\alpha]{\sum_{n=1}^{N} I_{h_n}{}^{\alpha}} \tag{11}$$

in which, I_{hn} is the magnitude of harmonic current from n-th harmonic source and α is summation exponent that its values are introduced in Table II for harmonic orders. Since there is no constraint for α at interharmonic orders in IEC 61000-3-6, it is assumed here that the α-exponent values for interharmonic frequencies (based on 5-Hz resolution) are the same as for harmonic frequencies.

It is expected that the values of resulting harmonic current (or total PE) at PCC calculated with IEC 61000-3-6 summation rule to be different from circuit model (or calculation model) and simulation model mentioned in sections IV-A,B; because the phase angle value is not considered in IEC summation rule [31]. Hence, by considering the phase angles of complex harmonic currents, the α-exponent values will also be different from its values introduced in IEC. To obtain updated α-exponent values and to compare it with its corresponding IEC values, a study based on complex harmonic current summation at PCC is performed for WPP of Fig. 6. Three different analysis methods are used and compared: (i) frequency-domain model (or circuit model) in which the contribution of each WT to the total complex harmonic current distortion at PCC is calculated based on each WT's PE TF. Then total PE at PCC is calculated based on summation of these contributions; (ii) time-domain model (or simulation model) in which the WPP presented in Fig. 6 is simulated in MATLAB/SIMULINK where different WT's operating points are considered. Then the PCC current is monitored and its harmonic spectrum (which contains a complex harmonic current for each harmonic or interharmonic order) is extracted; (iii) harmonic current source model (or IEC summation rule model) in which the contribution of 10-WTs to the total harmonic current distortion at PCC is calculated based on circuit models. Then the total PE at PCC is calculated based on (11). It is obvious that such a total PE obtained from this model has no imaginary part. It is worth mentioning that to study the harmonic summation based on models (i) and (iii), it is required to apply an input spectrum for each WT to calculate each WT contribution to total PE at PCC. Hence, 10 current spectrums of 50 monitored spectrums from the MV side of a type III WT transformer simulated in MATLAB/SIMULINK were selected. Current spectrums are monitored during 10 seconds covering whole WPP production range, and then DFT with sampling frequency of 256 times the power system frequency is applied to each 200 ms current waveform.

TABLE II

α-EXPONENT VALUES FOR HARMONIC AND INTERHARMONIC ORDERS BASED ON IEC 61000-3-6

Harmonic order	Interharmonic order	α-exponent value
$1<h<5$	$1.1<ih<4.9$	1
$5\leq h\leq 10$	$5.1\leq ih\leq 9.9$	1.4
$h>10$	$ih>10.1$	2

The spectrum of total harmonic current at PCC is shown in Fig. 14 for three above-mentioned models. The results of circuit and simulation models are very close to each other. There are some higher levels of harmonic current for IEC model occurred at harmonic orders 3, 5, 7, 23, 33, 35, and interharmonic orders 3.8, 4.2. The higher levels of harmonic current for circuit and simulation models occur at harmonic orders 3, 5, 7, 15, 23, 35, 37. A broadband amplification around 1750 Hz (orders 33, 35, 37) is due to resonance of PE TF. The emission level is almost the same for harmonic orders below 500 Hz for three models but the emission level for circuit and simulation models is lower than IEC model at interharmonic orders below 500 Hz. In general, emission levels obtained from IEC model are closer to those obtained from two other models at harmonic frequencies other than at interharmonic frequencies; although there are some exceptions: for example, the emission level at harmonic order 21 for IEC model is much higher than two other models whereas the emission level at harmonic orders 37, 41 for circuit and simulation models is much higher than IEC model.

Given the contribution of each WT (I_{hn}) and resulting magnitude for PCC harmonic current (I_h) and assuming the α values are unknown, Eq. (11) can be used to adjust α-exponent using Goal Seek tool in Excel. This tool, by defining α as a variable parameter, changes the α-values so that the right side of (11) is equal to PCC harmonic current of Fig. 14. This procedure is repeat for each harmonic and interharmonic frequencies in three above-mentioned models. The obtained values are plotted in Fig. 15. The solid-red line shows the IEC recommended values. The blue stem and orange curve show the adjusted α-exponent obtained from circuit model and simulation model respectively. It is obvious that all harmonic and interharmonic orders below order 5 tend to be aggregated with an exponent higher than

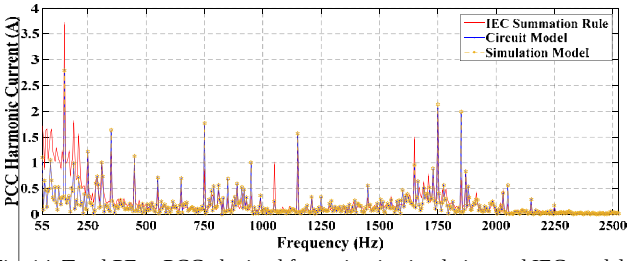

Fig. 14. Total PE at PCC obtained from circuit, simulation and IEC models.

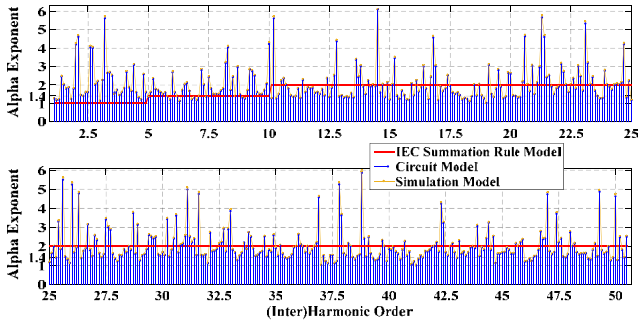

Fig. 15. Adjusted α-exponent. Upper: ih1.1-h25; lower: h25-ih50.5.

IEC-recommended value (i.e. 1). For orders between 5 and 10, the α-exponent value for most interharmonic orders is close to IEC-recommended value (i.e. 1.4). Most harmonic orders above 10 are aggregated with an exponent between 1.2 and 1.8 (that is an exponent lower than IEC-recommended value, i.e. 2). Higher α-exponent values are occurred at interharmonic frequencies. In general, it is concluded that the assignment of certain α value to the harmonic ranges specified in IEC 61000-3-6 is not possible.

VI. Conclusion

Due to shortcomings of the previous WPP models to study harmonic summation without the consideration of the DFAG converters model, an approach was adopted based on the average modelling of these converters and then the obtained impedance was added to the earlier model of TFs. By applying the DFAG impedance, the maximum value of TF is reduced and its corresponding resonance frequency is increased. The average modelling method does not affect the SE TA from the grid to WTs for frequencies above 500 Hz significantly, but it affects the PE TF considerably. The DFAG impedance resonance frequency is seen at 175 Hz in both PE TF and SE TA frequency response. Also, the updated TFs are applied to WPP's Norton model in order to adjust α-exponent in IEC 61000-3-6 summation rule. The results obtained from circuit and simulation models show that all harmonic and interharmonic orders below order 5 tend to be aggregated with an exponent higher than IEC-recommended value (i.e. 1). For orders between 5 and 10, the α-exponent value for most interharmonic orders is close to IEC-recommended value (i.e. 1.4). Most harmonic orders above 10 are aggregated with an exponent between 1.2 and 1.8 (that is an exponent lower than IEC-recommended value, i.e. 2). Higher α-exponent values are occurred at interharmonic frequencies.

References

[1] REN21 Secretariat. (2018). Renewables 2018: Global Status Report (GSR). Renewable Energy Policy Network for the 21st Century (REN 21). Paris, France. [Online]. Available: http://www.ren21.net/wp-content/uploads/2018/06/17-8652_GSR2018_FullReport_web_-1.pdf

[2] K. Yang, "Wind-turbine harmonic emissions and propagation through a wind farm," Licentiate thesis, Dept. Eng. Sci. and Math., Luleå Univ. Technol., Skellefteå, Sweden, 2012.

[3] C. Larose, R. Gagnon, P. Prud'Homme, M. Fecteau, and M. Asmine, "Type-III wind power plant harmonic emissions: field measurements and aggregation guidelines for adequate representation of harmonics," *IEEE Trans. Sustain. Energy*, vol. 4, no. 3, pp. 797-804, Jul. 2013.

[4] K. Yang, M. H. J. Bollen, E. O. A. Larsson, and M. Wahlberg, "Measurements of harmonic emission versus active power from wind turbines," *Elect. Power Syst. Res.*, vol. 108, pp. 304-314, Mar. 2014

[5] K. Yang and M. H. J. Bollen, "Interharmonic currents from a type-IV wind energy conversion system," *Elect. Power Syst. Res.*, vol. 143, pp. 357-364, Feb. 2017.

[6] S. A. Papathanassiou and M. P. Papadopoulos, "Harmonic analysis in a power system with wind generation," *IEEE Trans. Power Del.*, vol. 21, no. 4, pp. 2006–2016, Oct. 2006.

[7] B. Badrzadeh and M. Gupta, "Practical experiences and mitigation methods of harmonics in wind power plants," *IEEE Trans. Indust. App.*, vol. 49, no. 5, pp. 2279-2289, Sept.-Oct. 2013.

[8] M. Bradt *et al*, "Harmonics and resonance issues in wind power plants," in *Proc. IEEE PES T&D.*, Orlando, FL., USA, 2012, pp. 1-8.

[9] R. Zheng, M. H. J. Bollen, and J. Zhong, "Harmonic resonances due to a grid-connected wind farm," presented at the *14th ICHQP*, Bergamo, Italy, Sept. 26-29, 2010.

[10] K. Yang *et al*, "Decompositions of harmonic propagation in wind power plant," *Elect. Power Syst. Res.*, vol. 141, pp. 84-90, Dec. 2016.

[11] K. Yang, M. H. J. Bollen, and E. O. A. Larsson, "Aggregation and amplification of wind-turbine harmonic emission in a wind park," *IEEE Trans. Power Del.*, vol. 30, no. 2, pp. 791-799, Apr. 2015.

[12] K. Van Reusel and S. Bronckers, "Summation rule for wind turbines' harmonics challenged by measurements," presented at the *17th ICHQP*, Belo Horizonte, Brazil, Oct. 16-19, 2016.

[13] B. Badrzadeh *et al*, "Power system harmonic analysis in wind power plants—Part I: Study methodology and techniques," in *Proc. IEEE IAS Annu. Meeting*, Las Vegas, NV., USA, 2012, pp. 1–11.

[14] F. Ghassemi and K. L. Koo, "Equivalent network for wind farm harmonic assessments," *IEEE Trans. Power Del.*, vol. 25, no. 3, pp. 1808-1815, Jul. 2010.

[15] K. Yang, "On harmonic emission, propagation and aggregation in wind power plants," Ph. D. dissertation, Dept. Eng. Sci. and Math., Luleå Univ. Technol., Skellefteå, Sweden, 2015.

[16] L. Monjo, L. Sainz, J. Liang, and J. Pedra, "Study of resonance in wind parks," *Elect. Power Syst. Res.*, vol. 128, pp. 30-38, Nov. 2015.

[17] Ł. H. Kocewiak *et al*, "Wind turbine harmonic model and its application - Overview, status and outline of the new IEC technical report," presented at the *14th Int. Wind Integration Workshop*, Brussels, Belgium, Oct. 20-22, 2015.

[18] I. Vieto and J. Sun, "Sequence impedance modeling and analysis of type-III wind turbines," *IEEE Trans. Energy Convers.*, vol. 33, no. 2, pp. 537-545, Jun. 2018.

[19] L. Sainz *et al*, "Effect of wind turbine converter control on wind power plant harmonic response and resonances," *IET Elect. Power App.*, vol. 11, no. 2, pp. 157-168, Feb. 2017.

[20] F. Wang *et al*, "Modeling and analysis of grid harmonic distortion impact of aggregated DG inverters," *IEEE Trans. Power Electron.*, vol. 26, no. 3, pp. 786-797, Mar. 2011.

[21] F. D. Freijedo *et al*, "Harmonic resonances in wind power plants: modeling, analysis and active mitigation methods," in *Proc. IEEE PowerTech*, Eindhoven, Netherlands, 2015, pp. 1-6.

[22] Y. Song, X. Wang, and F. Blaabjerg, "Impedance-based high frequency resonance analysis of DFIG system in weak grids," *IEEE Trans. Power Electron.*, vol. 32, no. 5, pp. 3536-3548, May 2017.

[23] Y. Song and F. Blaabjerg, "Overview of DFIG-based wind power system resonances under weak networks," *IEEE Trans. Power Electron.*, vol. 32, no. 6, pp. 4370-4394, Jun. 2017.

[24] S. Y. Lui *et al*, "Aggregated DIFG wind farm harmonic propagation analysis," in *Proc. Congresso Brasileiro de Automatica*, Campina Grande, Brazil, 2012, pp. 1-8.

[25] E. Ebrahimzadeh *et al*, "Efficient approach for harmonic resonance identification of large wind power plants," in *Proc. IEEE PEDG*, Vancouver, BC., Canada, 2016, pp. 1-7.

[26] X. Xie *et al*, "A System-wide protection against unstable SSCI in series-compensated wind power systems," *IEEE Trans. Power Del.*, vol. 33, no. 6, pp. 3095-3104, Dec. 2018.

[27] Z. Miao, "Impedance-model-based SSR analysis for type 3 wind generator and series-compensated network," *IEEE Trans. Energy Convers.*, vol. 27, no. 4, pp. 984-991, Dec. 2012.

[28] I. Sowa *et al*, "Impedance-based analysis of harmonic resonances in HVDC connected offshore wind power plants," *Elect. Power Syst. Res.*, vol 166, pp. 61-72, Jan. 2019.

[29] A. Reznik *et al*, "LCL Filter design and performance analysis for grid-interconnected systems," *IEEE Trans. Indust. App.*, vol. 50, no. 2, pp. 1225-1232, Mar.-Apr. 2014.

[30] Ł. H. Kocewiak *et al*, "Resonance damping in array cable systems by wind turbine active filtering in large offshore wind power plants," I*ET Ren. Power Gen.*, vol. 11, no. 7, pp. 1069-1077, Jun. 2017.

[31] S. Tentzerakis, F. Santjer, J. Dirksen, and M. Baerschneider, "Methodology for the determination of the influence of the background harmonic voltage distortion on the measured harmonic currents of wind turbines and PV inverters," in *Proc. 1st International Conference on Large-Scale Grid Integration of Renewable Energy in India*, New Delhi, India, 2017.